High-Spatial Resolution Giant Magnetoresistive Sensors – Part II: Application in Biomedicine

C.P. Gooneratne[1], K. Chomsuwan[2], M. Kakikawa[3], and S. Yamada[3]

[1] King Abdullah University of Science and Technology,
Thuwal, Saudi Arabia
Chinthaka.Gooneratne@kaust.edu.sa
[2] King Mongkut's University of Technology Thonburi,
Bangkok, Thailand
[3] Kanazawa University, Kanazawa, Japan

Abstract. Magnetic fluid based hyperthermia therapy for treating cancerous tumors can be performed with a high success rate and minimal error given the possibility of detecting and estimating magnetic fluid weight density *in vivo*. In this chapter, a uniquely designed GMR needle probe is presented for the detection and estimation of magnetic fluid content density inside tumors. Experimental results showed that the proposed technique has a good potential to be implemented in hyperthermia therapy in the future.

1 Introduction

Magnetic fluid based hyperthermia has the potential to be an effective, non-invasive cancer therapy with negligible side effects [1-8]. Magnetic fluid is injected into the affected area and an external AC magnetic flux density is applied to exploit the self-heating properties of the magnetic beads (MBs) in the fluid. Temperatures in excess of 42 °C destroy tumors [9-12]. Generally, all parameters, except the magnetic fluid content density *in vivo*, are known in the specific heat equation which governs the heat given in hyperthermia therapy to destroy cancer cells. This is due to the fact that magnetic fluid injected into an affected area spreads to neighboring tissue thus, effectively reducing the magnetic fluid content density. Hence, accurate estimation of magnetic fluid content density *in vivo* is critical for successful cancer treatment by hyperthermia therapy. The purpose of this research is to develop a method and appropriate apparatus/tools to estimate magnetic fluid content density *in vivo* so that tumors can be destroyed without affecting healthy cells. The key feature of this research is the fabricated novel GMR needle probe. The GMR needle probe is designed in such a way so that it can be inserted *in vivo* in a minimally-invasive way to detect and estimate magnetic fluid content density.

2 Estimation of Magnetic Fluid Density Inside Tumors

2.1 Introduction

Recent cancer treatment has focused on the effectiveness of killing localized or deep seated cancer tumors. The use of magnetic materials to heat tumors was first proposed

C. Reig et al.: *Giant Magnetoresistance (GMR) Sensors*, SSMI 6, pp. 243–273.
DOI: 10.1007/978-3-642-37172-1_10

by Gilchrist et al in 1957 [13], who used iron oxides to heat lymph nodes. Since then much research has been done to heat tumors directly in a non-invasive way. In the past, heating methods were difficult, expensive and unsafe resulting in the whole procedure being unfeasible. However, hyperthermia therapy with the aid of magnetic fluid is now regarded as one of the most promising cancer therapies due to the progress made in the synthesis of superparamagnetic type beads in the last decade. Superparamagnetic type MBs have single domains, where the magnetization direction flips randomly due to temperature [14]. However, when an external magnetic flux density is applied the magnetization direction aligns in the direction of the applied flux; therefore, MBs can be controlled by an external magnetic flux density [15, 16]. In the case of magnetic fluid hyperthermia, MBs can be injected *in vivo* and moved to the target site, held there until treatment is completed and removed afterwards, by localized magnetic flux gradients. Furthermore, since MBs have large surface to volume ratios for binding of biological cells and are physiologically well tolerated there are limitless opportunities for their utilization in many biomedical applications such as biological cell tagging, targeted drug delivery and MRI [17-20]. Magnetite (Fe_3O_4) is the most widely used and promising MB available today for biomedical applications [21-23]. Fe_3O_4 beads have hydrophobic surfaces and when they interact with each other the beads agglomerate to form clusters which increase the bead size. Hence, to stabilize MBs and prevent agglomeration a stabilizer such as a surfactant or polymer is usually added during preparation [21-25].

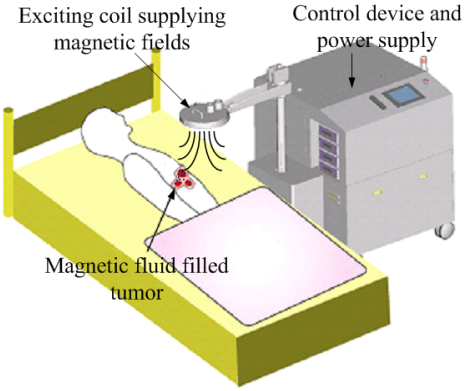

(a) Hyperthermia therapy system

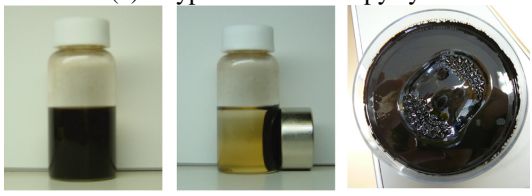

(b) Magnetic fluid

Fig. 1. Magnetic fluid hyperthermia

Cancer cells are different to normal, healthy cells in many ways including how they react to heat [26]. Due to this difference it is possible for hyperthermia therapy to destroy without harming the healthy normal cells surrounding the tumor. Figure 1 (a) shows a magnetic fluid hyperthermia therapy system. As shown in Fig. 1 (b), magnetic fluids used in hyperthermia therapy are colloidal mixtures consisting of MBs suspended in a carrier fluid, usually an organic solvent or water; the fluid is injected directly into the tumor body or into an artery supplying the tumor. An external AC magnetic flux density of several kHz is then applied to the magnetic fluid filled area of the body. For biomedical purpose, the frequency has to be to 50 kHz to avoid neuromuscular electrostimulation and lower than 10 MHz for appropriate penetration depth of the radio frequency field [27]. Heat is produced in the magnetic fluid filled tumor since it is exposed to an external AC magnetic flux density. The heating losses of MBs are mainly due to Nèel relaxation and Brownian motion [28, 29]. Most types of cancer cells are more sensitive to temperatures in excess of 42° C than normal cells. Tumor apoptosis can be triggered if the temperature can be controlled at the therapeutic threshold of 42° C for a prolonged period of time, resulting in the tumor being destroyed or at least partly destroyed. Since the energy is coupled magnetically to the MBs, bone or boundaries of different conductive tissues do not interfere with power absorption as with electric field dominant systems used for regional hyperthermia for example [30]. Furthermore, there is also homogenous heating in the target region since even though there is a large number of MBs, each can be thought of as a separate hot source, giving temperature homogeneity during inactivation of cancer cells [31]. So, given that the fluid can be injected homogenously throughout the target region a homogenous cell inactivation could be expected. The AC magnetic flux density should also be homogenous because each bead has its specific power absorption, which is only constant if the applied magnetic flux density is also homogenous.

The specific heat capacity Q (W/ml), generated by magnetic fluid can be calculated as follows [32]:

$$Q = k_m f D_w B^2, \tag{1}$$

where k_m is a constant of 3.14×10^{-3} (W/Hz/(mgFe/ml)/T^2/ml), f is the exciting frequency of the applied magnetic flux density (kHz), D_w is the magnetic fluid weight density (mgFe/ml) and B is the amplitude of the applied magnetic flux density (T).

Currently, one of the main problems associated with magnetic fluid hyperthermia is that the magnetic fluid spreads inside tissue once injected, reducing D_w. From Eq. 1 it can be seen that Q is directly proportional to D_w. Inaccurate estimation of D_w has two major effects: i) if a low dosage is given the overall effect is thermal underdosage in the target region which often leads to recurrent tumor growth, ii) if heat given to a target region exceeds the therapeutic limit it may damage healthy cells. Hence, it can be stated that the quality of magnetic fluid hyperthermia treatment is proportional to the accuracy of estimating D_w *in vivo*. The purpose of this research is to develop a method and appropriate apparatus/tools to estimate D_w *in vivo* before hyperthermia therapy. The key feature of this research is the fabricated unique GMR needle probe which is designed in such a way so that it can be inserted *in vivo* in a minimally invasive way to detect and estimate D_w.

2.2 Analytical Estimation of Magnetic Fluid Parameters

2.2.1 Relationship between Relative Permeability, Magnetic Fluid Weight and Volume Density

The different variables used in this relationship are defined as follows:

D_v: (measured as a percentage); magnetic fluid volume density
D_w: (measured as weight per volume); magnetic fluid weight density
γ_f: (W-35 sample – Taiho Co. = 4.58); specific gravity of MBs

So then, the relationship between D_v and D_w can be expressed as follows:

D_w: weight of MBs in 1 ml volume : weight of combined MBs and water in 1 ml volume

$$D_w = \frac{(\gamma_f \times D_v)}{((1 - D_v) + \gamma_f \times D_v)}. \tag{2}$$

This can be simplified to,

$$D_v \approx D_w / \gamma_f . \tag{3}$$

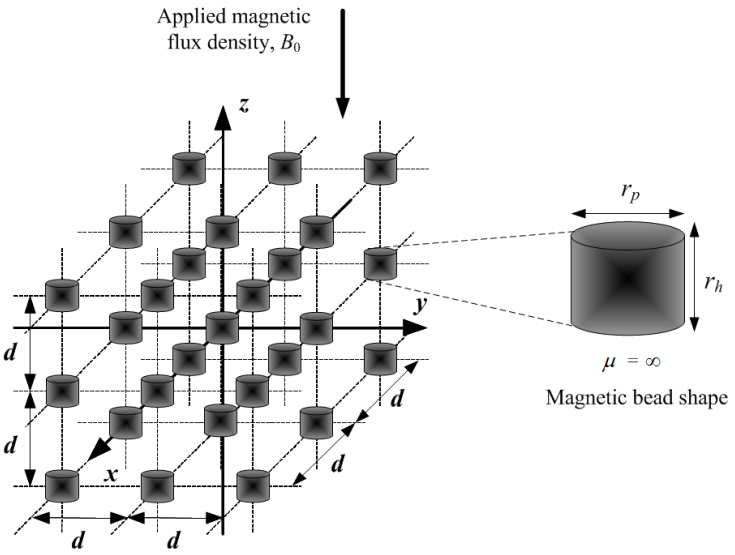

Fig. 2. Model of MBs uniformly distributed inside magnetic fluid

The relative permeability (μ^*) of magnetic fluid can be estimated by measuring the magnetic flux density in tissue injected with magnetic fluid. It is assumed that the MBs are cylindrical in shape with equal height (r_h) and diameter (r_p), and that they are uniformly distributed in the fluid as shown in Fig. 2. It is also assumed that μ^* of MBs is infinite and water is one. The permeance of the magnetic fluid based on an equivalent magnetic path is thus estimated from the assumptions [33]. Permeance generally refers to the degree to which a material admits a flow of matter or energy. D_w can be estimated based on the prediction of the magnetic flux path when magnetic fluid is placed under a uniform magnetic flux density. Due to the existence of MBs with infinite permeability the magnetic circuit for the external magnetic flux changes as shown in Fig. 3. When considering the permeance through MB magnetic flux lines will converge as shown in Fig. 3 (a). Hence, we take into account the surface area of the magnetic flux path. It is assumed that the diameter of the magnetic flux path surface area is twice the cylindrical bead diameter. Two equivalent magnetic paths, with and without magnetic nabeads are considered. The volume of the cylindrical MB, given that $r_p = r_h$, is

$$V_m = \frac{\pi r_p^3}{4}. \tag{4}$$

D_v = volume of MB : total volume

$$D_v = \frac{\pi r_p^3}{4} \div d^3 = \frac{\pi r_p^3}{4d^3}. \tag{5}$$

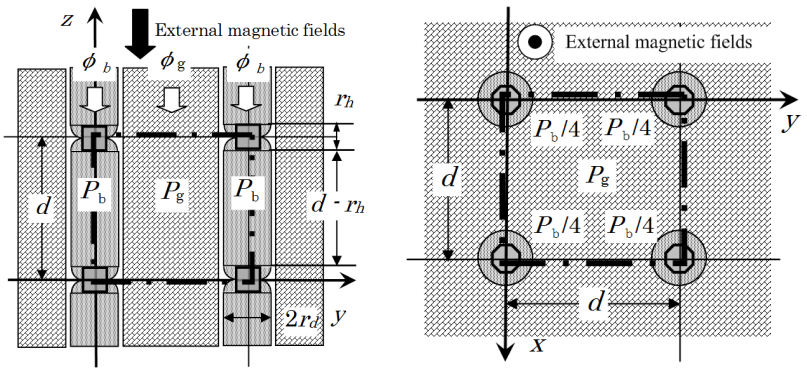

(a) Side view of magnetic circuit path.

(b) Top view.

Fig. 3. Equivalent magnetic circuit path of magnetic liquid under a z direction external magnetic flux density

Equation (5) can be rearranged to obtain

$$d = \left(\frac{\pi}{4D_v} \right)^{1/3} r_p. \tag{6}$$

The permeances of two magnetic paths are expressed as follows:

The permeance of the magnetic path through MB is given by

$$P_b = \frac{\mu_0 \pi r_p^2}{d - r_p} \approx \frac{\mu_0 \pi r_p^2}{d} \left(1 + \frac{r_p}{d} \right). \tag{7}$$

The permeance of the magnetic path through liquid is given by

$$P_g = \frac{\mu_0 \left(d^2 - \pi r_p^2 \right)}{d}. \tag{8}$$

Based on equations (7) and (8), the permeance per unit volume can be derived as

$$P = \frac{\mu S}{l} = \frac{\mu_0 \mu_s 1^2}{1} = \mu_0 \mu_s = \left(P_b + P_g \right) \left(\frac{1/d^2}{1/d} \right) = \frac{P_b + P_g}{d}. \tag{9}$$

Equation (9) can be expanded as follows:

$$\mu_0 \mu^* = \frac{1}{d} \left[\frac{\mu_0 \pi r_p^2}{d} \left(1 + \frac{r_p}{d} \right) + \frac{\mu_0 \left(d^2 - \pi r_p^2 \right)}{d} \right],$$

$$\mu_0 \mu^* = \mu_0 \left[\frac{\pi r_p^3}{d^3} + 1 \right]. \tag{10}$$

Relative permeability of magnetic fluid can then be expressed as

$$\mu^* = 1 + \frac{\pi r_p^3}{d^3}. \tag{11}$$

Substituting equation (6) into (11), for $D_v << 1$, we obtain

$$\mu^* = 1 + 4D_v. \tag{12}$$

Then, substituting equation (3) into (12) the following equation, for $D_w << 1$, is obtained.

$$\mu^* = 1 + 4D_w / \gamma_f. \tag{13}$$

Equation (13) shows that μ^* of magnetic fluid is directly proportional to D_v and D_w. Furthermore, the shape and/or size of the MBs have no effect on μ^* of magnetic fluid.

Assuming the same equivalent path the equivalent μ^* has the same expression even though the bead could be of spherical shape. This expression holds on the condition that the cavity includes a small amount of MBs.

The electron microscopy of the magnetic fluid shows that the MBs have a cluster structure as shown in Fig. 4 (a). It was then assumed that the cluster of magnetite is distributed uniformly as shown in Fig. 4 (b). It can be seen that there is some space between the magnetite beads in the cluster model, so we considered the space factor of spherical magnetite h_s. So then the effective specific gravity can be expressed as

$$\gamma_f{}' = h_s \gamma_f . \tag{14}$$

where h_s is 0.523.

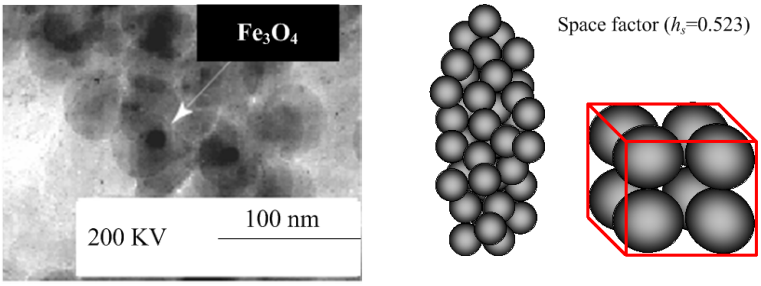

(a) Electron microscopy image of magnetic fluid.

(b) Spherical type model of magnetite.

Fig. 4. Cluster structure of magnetic nanoparticles

Equation (13) can then be written as

$$\mu^* = 1 + 4D_w / h_s \gamma_f . \tag{15}$$

which, in general terms can be written as

$$\mu^* = 1 + C_d D_w / h_s \gamma_f . \qquad (D_w << 1) \tag{16}$$

where C_d is a coefficient which is theoretically 4 [34-36].

Equation (16) relates μ^* of magnetic fluid to D_w. To confirm equation (16) experimental analysis was carried out with the aid of a vibrating sample magnetometer (VSM). Hysteresis curves were obtained for magnetic fluid samples with different weight densities. Figure 5 shows the comparison of the experimental and theoretical results. It can be seen that μ^* is proportional to D_w. The theoretical and experimental results are also in good agreement.

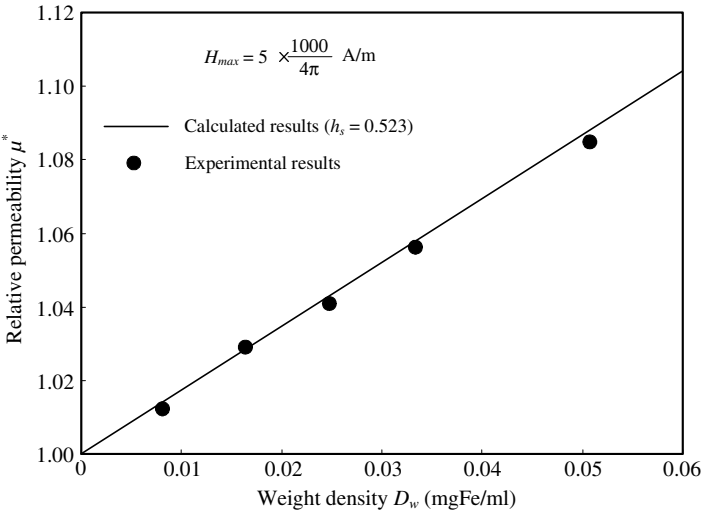

Fig. 5. Relationship between relative permeability and magnetic fluid

2.2.2 Estimation of Magnetic Fluid Weight Density by Measuring Magnetic Flux Density Inside and Outside a Magnetic Fluid-filled Cavity

Consider the situation shown in Fig. 6. An ellipsoidal cavity filled with magnetic fluid is placed under a uniform magnetic flux density. Given that the outside environment is air with $\mu^* = 1$, and magnetic fluid has μ^* slightly greater than 1, magnetic flux lines will converge and concentrate at the magnetic fluid filled ellipsoidal cavity. If a magnetic flux density B_0, is applied then the magnetic flux density in the cavity can be assumed as B_1. The magnetic flux density inside the magnetic fluid filled cavity B_1, will change according to D_w. The magnetic flux density at the center of the cavity B_1, can be expressed according to the following equation [37].

$$B_1 = \frac{B_0}{\frac{\mu_0}{\mu} + N\left(1 - \frac{\mu_0}{\mu}\right)}, \tag{17}$$

$$B_1 - B_0 = \frac{\mu^*}{1 + N\left(\mu^* - 1\right)} B_0 - B_0 = B_0\left(\frac{\mu^*}{1 + N\left(\mu^* - 1\right)} - 1\right), \tag{18}$$

$$\frac{B_1 - B_0}{B_0} = \left[\left(1 - N\right)\left(\mu^* - 1\right)\right] \qquad (\mu^* \approx 1) \tag{19}$$

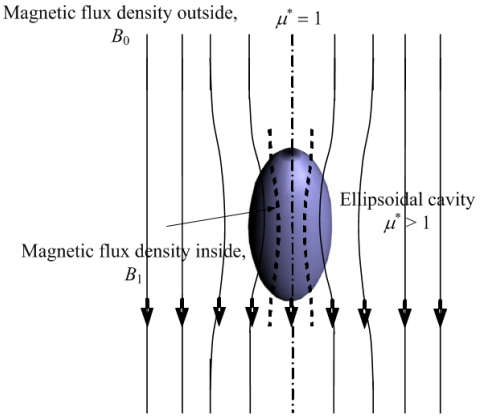

Fig. 6. Magnetic fluid filled ellipsoidal cavity under the influence of a uniform magnetic flux density

Substituting equation (16) into (19) we obtain the change in magnetic flux density (δ) as shown below.

$$\delta = \frac{B_1 - B_0}{B_0},$$

$$\delta = \frac{C_d (1 - N) D_w}{(h_s \gamma_f)}. \tag{20}$$

It can be seen from equation (20) that D_w can be effectively calculated from the difference between B_1 and B_0. The change in magnetic flux density is directly proportional to D_w. However, the demagnetizing factor N, which depends on the shape and size of cavity, influences the estimation of D_w.

2.3 GMR Needle Probe

2.3.1 Design of the GMR Needle Probe

The fabricated GMR needle probe as shown in Fig. 7 (a) is unique in the sense that it can be applied inside the body in a low-invasive way. The needle detection part is shown in Fig. 7 (b). The needle length is 20 mm, where 15 mm is available for insertion inside the body, and approximately 310 μm in diameter. Generally, such a fine needle can be expected to break easily due to its lack of rigidity. However, since the substrate itself is cut into a needle shape, a hard material such as aluminum titanium carbide (AlTiC), a sintered material of aluminum oxide (Al_2O_3) and titanium carbide (TiC), can be used as the base material to make the needle strong. The needle-shaped detecting part consists of a substrate to which a cutting process is applied to have a needle shape, four GMR elements formed of thin films on the surface of the substrate, four connection/bonding pads, lead conductors for electrically connecting the GMR

elements to the connection/bonding pads and a protection film for covering the GMR elements and lead conductors, except parts of the connection/bonding pads. The GMR sensors, connection/bonding pads and lead conductors are formed on a wafer by a wafer process utilizing thin film photolithography techniques. After, a machining process is used to cut the wafer to a needle shape. The substrate is made of AlTiC. The GMR elements used in the needle have a spin-valve structure. The spin-valve structure consists of an antiferromagnetic layer that is used to fix or pin the magnetization of the pinned ferromagnetic layer, a non-magnetic space layer and a free layer of ferromagnetic material where the magnetization is free to move in response to an applied magnetic flux density. The magnetization direction of the pinned layer is perpendicular to the free layer and same in all of the four spin valve GMR elements. The connection/bonding pads and the lead conductors are made of copper (Cu). These connection/bonding pads are formed by a bump layer of Cu, and a bonding pad layer of gold (Au) that is laid on the bump layer.

The novel idea of the GMR needle probe is the GMR sensing area (75 ×45 μm) present at the tip of the needle. MBs are used *in vivo* as self-heating agents for hyperthermia treatment; accurate measurement of MB density is very important for successful treatment. When a uniform external magnetic flux density is applied to an area filled with MBs the flux lines will converge to this area (because the MBs make the relative permeability (μ^*) of this area slightly more than one) resulting in a change in magnetic flux between the applied flux and the flux at the target area. In such a case the GMR needle probe can be inserted into the target area in a minimally invasive

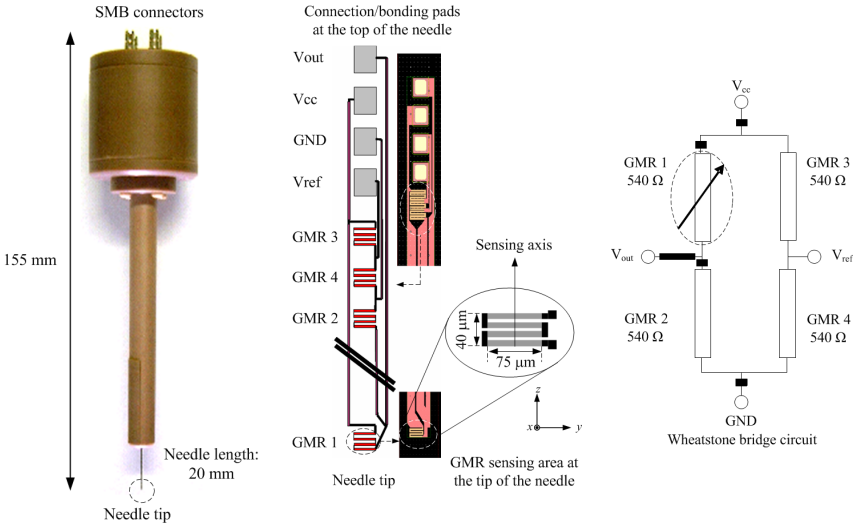

(a) Fabricated GMR needle probe.

(b) Needle design.

(c) Wheatstone bridge design of sensors.

Fig. 7. GMR needle probe

pattern to measure the magnetic flux density inside as well as outside the area. One of the main features of the GMR needle probe is the way the Wheatstone bridge circuit is designed as shown in Fig. 7 (c). There is a sensing area at the tip which is part of a Wheatstone bridge circuit with four other GMR sensing areas 20 mm further up, near the connecting/bonding pads. This means that rather than measuring the magnetic flux density inside and outside separately the GMR needle probe has the ability to measure both these quantities simultaneously.

2.3.2 Characterization of GMR Needle Probe

The DC characteristics of the GMR needle probe are shown in Fig. 8 for a magnetic flux density range of -12 to 12 mT. The DC characteristics of the GMR probe show that the maximum magnetic ratio is approximately 13.30 %. The linear region sensitivity of the GMR needle probe is around 2.5 %/mT. There is a very low hysteretic loop. It can be seen from the figure that the GMR needle probe has high sensitivity for applied magnetic flux density in the range of -1 to 1 mT.

Two types of experiments were performed to obtain the AC small signal characteristics of the GMR needle probe. Since the research performed involves AC magnetic flux the investigation of small signal AC characteristics of the GMR needle probe is very important.

Experiment 1: Measurement with Lee-Whiting coil

A Lee-Whiting coil was used to produce a magnetic flux density of 0.1 mT at 100 Hz as shown in Fig. 9 (a). The current to the coils are provided by the function generator through the high speed power amplifier. The output through V_{out} in the GMR needle probe Wheatstone bridge was sent to the oscilloscope which in turn was sent to a computer by GPIB for analysis. During experiments a current of 5 mA was fed to the

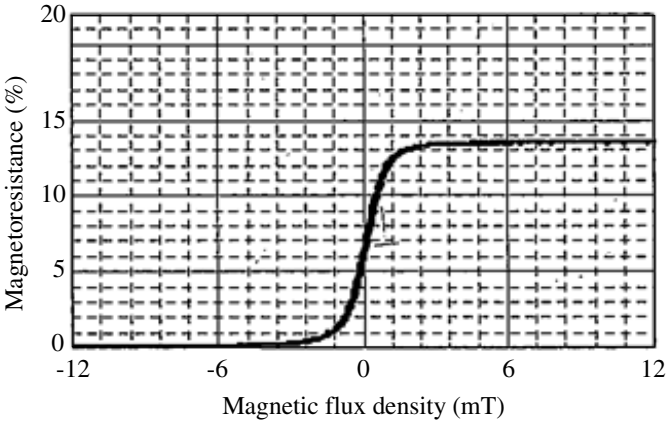

Fig. 8. DC characteristics of the GMR needle probe

GMR needle probe. The GMR needle probe was also tested for three different directions, *x*, *y* and *z*. Fig. 9 (b) shows the sensitivity results for all three directions. It can be seen that the response in the *x* and *y* direction is very low compared to the *z* direction. This can be explained by the fact that the sensing axis of the GMR sensing element at the needle tip is parallel to the magnetic flux density, which is in the *z* direction. The sensitivity in the *z* direction is approximately 13 mV/mT.

Experiment 2: Measurement with gradient distribution of magnetic flux density

The experimental setup is shown in Fig. 9 (c). Two coils are used with current flowing in parallel with respect to each other. This results in a magnetic flux density of zero at the center of the coils. The methodology for these experiments is based on the distance between the GMR sensing area at the tip of the needle and the other three GMR sensing areas near the connection/bonding pads. The distance between the GMR sensing area at the tip and the other three sensing areas is 20 mm. The magnetic flux density that is produced by parallel coils follows a gradient pattern. So the gradient at 20 mm can be obtained and used to calculate the AC sensitivity of the sensor. The gradient can be adjusted by the current to the coil which is proportional to the magnetic flux density. Since the magnetic flux density is zero at the center the GMR sensing areas near the connection/bonding pads can be placed there. The GMR sensing area at the tip can be placed where there would be a magnetic flux density and the Wheatstone bridge output (V_{out} - V_{ref}) can be obtained. The change of the signal will be solely due to the GMR sensing area at the tip. A current of 5 mA was fed to the GMR needle probe and a gradient of approximately 0.003.6 mT/20 mm was given by the two parallel coils. The frequency of the exciting current fed to the two parallel coils by the function generator through the high speed power amplifier was 100 Hz. The V_{out} and the V_{ref} signals were connected to a digital lock-in amplifier (NF electronics LI5640). The lock-in amplifier was used to analyze the results. The results showed that for AC small signal characterization at 100 Hz the sensitivity of the sensor is 15.3 mV/mT. Hence, for small signal characterization at 100 Hz the sensitivity of the sensor is between 13-15 mV/mT.

2.4 Estimation of Magnetic Fluid Weight Density Using the GMR Needle Probe

2.4.1 Experimental Methodology

In explaining the experimental method of estimating D_w (theoretically outlined in section 2.2.2), Fig. 10 is taken into account. Consider the event where the tip of the needle is inserted into the center of a tumor cavity under a uniform magnetic flux density (B_0). The four GMR sensors are exposed to B_0, assuming that the cavity is empty ($\mu^* = 1$ can be assumed inside and outside the cavity). So there is no change in magnetic flux density inside and outside the cavity since B_1 is equal to B_0. However, when the tumor cavity is filled with magnetic fluid, μ^* inside is greater than outside the cavity. Hence, the GMR sensing area at the tip of the needle is exposed to a

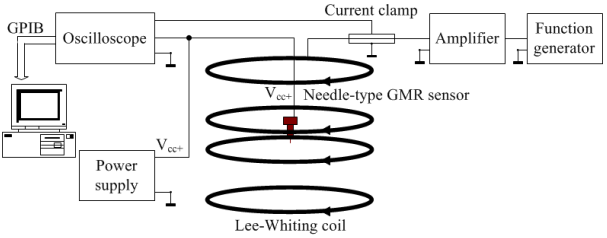

(a) Experimental set up for AC small signal characteristics.

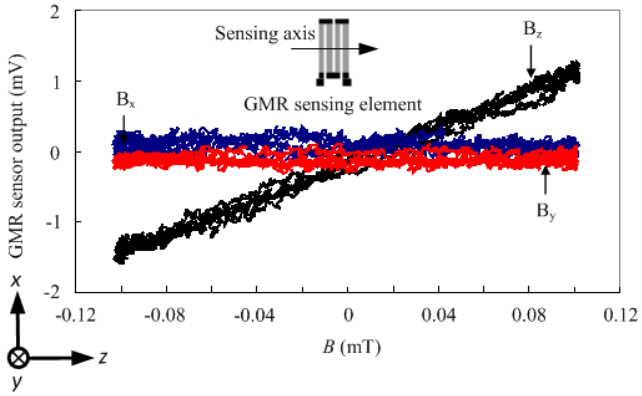

(b) AC small signal characteristics of the GMR needle probe (Section 2.3.2, Experiment 1).

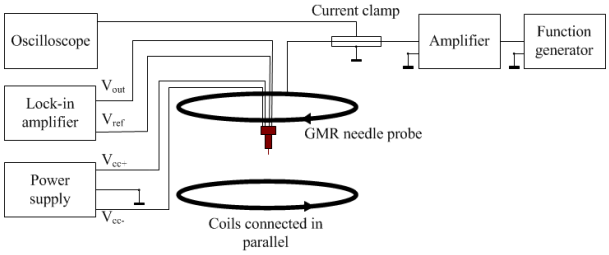

(c) Experimental setup for small signal AC characterization with gradient distribution of magnetic flux density (Section 2.3.2, Experiment 2).

Fig. 9. Small signal AC characterization at 100 Hz

magnetic flux density B_1, which is higher than the applied magnetic flux density B_0. However, since the other three sensors are located further up near the bonding pads, and hence outside the magnetic fluid filled cavity, they will still be exposed to the applied magnetic flux density. This way, B_1 and B_0 can be measured simultaneously. As explained in section 2.2.2, D_w is proportional to the differential magnetic flux density inside and outside a magnetic fluid filled cavity; thus, D_w can be estimated from the change in B_1 and B_0.

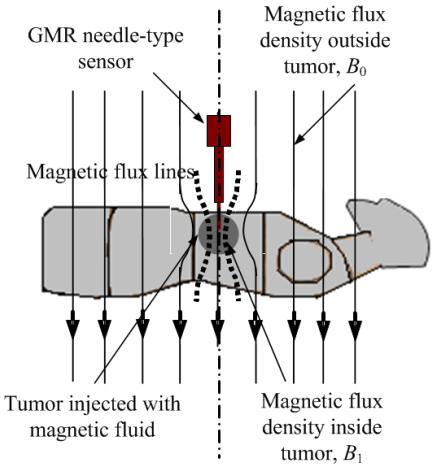

Fig. 10. Magnetic fluid filled tumor under a uniform magnetic flux density

One of the main requirements for the accurate estimation of D_w using the GMR needle probe is a uniform magnetic flux density. Helmholtz coils are used in a variety of applications, primarily due to its ability to produce a uniform magnetic flux configuration, ease of construction and flexibility. The accuracy of the relative magnetic flux density produced depends on how precise the Helmholtz coils are constructed and how accurate the current through them is maintained [38]. A lot of research has been done to find optimum parameters for designing super uniform Helmholtz coil systems [39-42]. A Helmholtz coil system consists of two coils, either circular or square, of equal radius and equal number of turns along an axis through the center of the coils, separated by a distance equal to the radius of the coils. The total magnetic flux produced is the sum of the two coils. A large volume of magnetic flux uniformity based around the mid-point between the two coils can be explained by the good deal of cancellation for the off-axis flux components generated by the coil. Magnetic flux density is generated by currents. A static flux will be produced if the currents are unchanging (DC). However for a changing current the flux will vary and will not only have magnetic, but also electric and electromagnetic components. Influence of fields other than magnetic increases when the operating frequency rises. However high frequency effects can be ignored if the operating frequency is kept low enough. In this region generally known as the "quasi-static" region, the differences between the flux generated by DC and AC can be assumed negligible. The Helmholtz coil has many applications in a variety of areas such as, calibration of magnetic instruments and probes, biomedical/bioelectromagnetic studies, diagnostic studies on electron beams, and in the study of the magnetic properties of materials [43-46].

In this research it is essential that the specifications required for the area of uniformity for experiments is explicitly met. A common error when designing a Helmholtz coil system is the assumption that the magnetic flux density will be uniform. This is true only for a certain volume around the center. Improvements and modifications are needed to improve the region of uniformity. A Helmholtz coil system was designed to obtain a uniform magnetic flux density with an error ≤ 0.01 % for 0.03m in the radial

(r) and axial (z) axes, for the experiments performed in sections 2.4.2 and 2.4.3. If a standard one coil pair is used the common radius of the system would be quite large for the required specifications. A large number of coil designs such as Maxwell tri-coil, Lee-Whiting, Alldred-Scollar and Rubens coil, have been reported [40]. However, for our specifications and experimental setup a planar coil system consisting of three coil pairs was chosen as the ideal system [47]. The coil design is shown in Fig. 11 (a). The three coil pair system is used to produce a magnetic flux density of B_0. The flux density will concentrate at the magnetic fluid filled cavity. The GMR needle probe is placed at the center of the cavity, hence the center of the common axis between the three coil pairs. The magnetic flux in the cavity can be assumed as B_1. B_1 changes with D_w. As explained before the change in B_1 and B_0 is proportional to D_w. It is critical that the magnetic flux distribution in this region should have an error of less than or equal to 0.01 % with respect to the center of the coils, because the percentage change in magnetic flux density for the magnetic fluid weight densities used for experiments is in the order of 1/10. So it is essential that the experimental area is more uniform to eliminate ambiguity in experimental results. The analytical results for the Helmholtz tri-coil are shown in Fig. 11 (b); it can be seen that the fluctuation of magnetic flux density is less than or equal to 0.01 %, 0.03 m in the axial and radial direction from the midpoint. The darker the region in the contour plot, the more uniform it is. The fabricated Helmholtz tri-coil is shown in Fig. 11 (c).

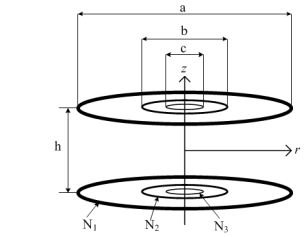

a = 770 mm (diameter of coil 1) N_1 = 140 (number of turns in coil 1)
b = 260 mm (diameter of coil 2) N_2 = 4 (number of turns in coil 2)
c = 214 mm (diameter of coil 3) N_3 = 1 (number of turns in coil 3)

h = 315 mm height between upper and lower sets of coils

(a) Helmholtz tri-coil design.

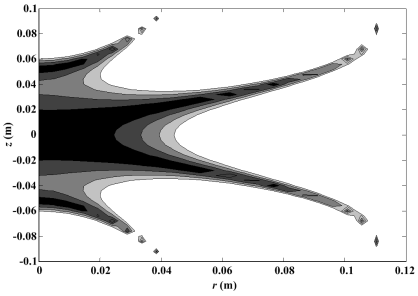

(b) Contour error plot (≤ 0.01 % variation of magnetic flux density from the center of the coil).

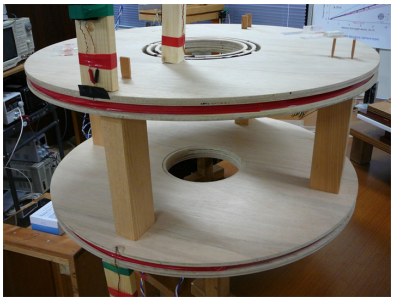

(c) Fabricated Helmholtz tri-coil.

Fig. 11. Helmholtz tri-coil

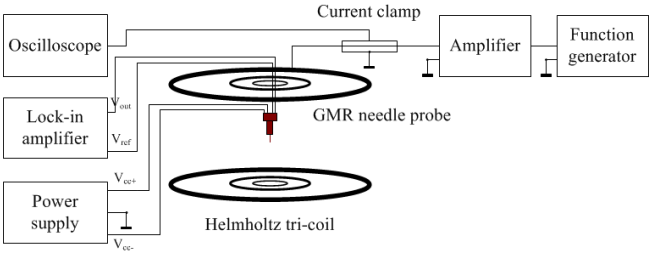

(a) Block diagram.

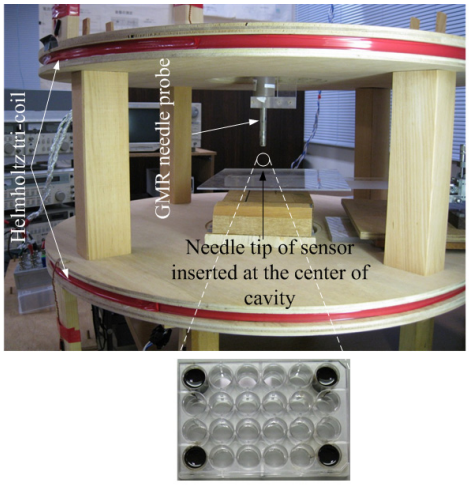

Tray with embedded magnetic fluid filled cavity

(b) Experimental apparatus.

Fig. 12. Experimental setup

Figure 12 shows the experimental setup for estimating low-concentration magnetic fluid inside plastic cylindrical containers. Low-concentration magnetic fluid can be defined by the content densities used in clinical applications. Magnetic fluid weight densities used for clinical applications are typically less than 2.8 % and potentially decreases even more when injected *in vivo*, due to spreading inside tissue. Hence, magnetic fluid of original D_w 40 % was thinned by mixing with distilled water. Plastic trays with embedded cavities (s = 0.625) were filled with thinned fluid of various densities. The fabricated Helmholtz tri-coil was used to produce a uniform magnetic flux density of 0.1 mT at 100 Hz (0.01 % fluctuation 0.03 m in the axial and radial direction from center of the coil). Current of 267 mA was provided to the coils of the Helmholtz tri-coil by a function generator (Sony Tektronix AFG310) through a high speed power amplifier (NF Electronics 4055). A current clamp (Hioki 3274) was clamped to the coils carrying current to the Helmholtz tri-coil and connected to an oscilloscope (Yokogawa DL4100) to analyze the current waveform. Additionally, a Gauss meter (MTI mm-340) was also used to confirm the magnetic flux density at the

center of the Helmholtz tri-coil. A constant current of 5 mA was given to the GMR needle probe by a DC power supply (Matsusada Precision Instruments).

The GMR needle probe was inserted as shown in Fig. 12 (b). The GMR needle probe tip was placed in the middle of the Helmholtz coil and the cylindrical cavity was moved so that the needle tip was at the center of the cavity. The GMR needle probe was then used to estimate the D_w of the thinned magnetic fluid, by measuring the applied magnetic flux density (B_0 = 0.1 mT) and the magnetic flux density inside (B_1) thinned magnetic fluid filled cavities. The bridge output voltages across the GMR needle probe were measured by a lock-in amplifier (NF Electronics LI5640). By applying the results to equation (20), the change in magnetic flux density was obtained for all the cavities with different thinned magnetic fluid weight densities. The experimental results are shown in Fig. 13. The figure denotes the relationship between D_w and the change ratio of magnetic flux densities. When the cavity is thin and long (N = 0), the relationship shows the upper limit. The demagnetizing factor N for an elliptic body depends on the shape ratio of the cavity s, as shown in the figure. For spherical shaped cavities s = 1 and N = 1/3, and for flat shaped cavites s = 0.5 and N = 0.527. It can be seen from the experimental results that D_w is proportional to change in magnetic flux density and the results fall between theoretical lines for long and flat ellipsoidal cavities.

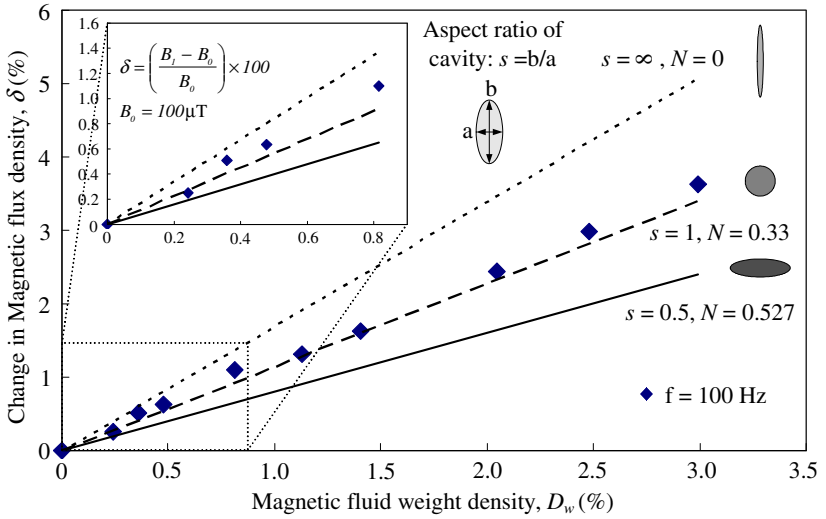

Fig. 13. Estimation of magnetic fluid weight density in a tray with embedded cavities

2.4.2 Detection and Estimation of Low Concentration Magnetic Fluid Inside Tumor-Simulating Cylindrical Agar Cavities

The evaluation of cancer staging is generally done with respect to the size of the tumor. The tumor, node, metastasis (TNM) staging system is commonly accepted for the evaluation of pathological stage [48]. Assuming that tumors are spherical in

shape, the cutoff diameters for the different stages depend on the type of tumor. Generally tumors are classified into 5 stages (T0 – T5). In the T0 stage there is no evidence of a primary tumor but is defined as carcinoma in situ (CIS). This means that malignant cells that arise from epithelial cells have not invaded surrounding tissue. Recent studies have shown that the general cut off point between T1/T2 and T3 tumors is 50 mm [49, 50]. In T1 tumors diameters are not more than 20 mm and localized to one part of the body. In T2 tumors cancers are locally advanced and diameters vary between 20 and 50 mm. In later stage (T3 and T4) tumors the diameters are more than 50 mm, and also the cancer has started to spread into surrounding tissue, lymph nodes and body organs. Ideally hyperthermia therapy is performed on non-invasive, in situ tumors which are normally detected when they are small and confined [51]. In these cases (tumor diameter less than 20 mm) the cancer has not spread to other organs. Low-concentration magnetic fluid (less than 2.8 % D_w) is generally used in hyperthermia therapy, to keep the dose *in vivo* as low as possible. However, once injected the magnetic fluid tends to spreads inside tissue, further decreasing the low-concentration D_w. The specific heat capacity required to destroy a tumor is proportional to AC magnetic flux density amplitude, frequency and D_w. Specific heat capacity is also clearly correlated with therapeutic outcome since it can only be increased up to a certain critical value to avoid heating of healthy tissue. Hence, it is vital that D_w be known *in vivo* before as well as after treatment (to check for remnant density). This section provides details about a novel GMR needle probe that can be inserted *in vivo* in a low-invasive way to detect and estimate low-concentration D_w in T1 tumors for successful implementation of hyperthermia therapy.

To simulate the situation of detecting magnetic fluid inside the body, cylindrical agar pieces (simulating tumors) were injected with thinned magnetic fluid of various densities and immersed in potato starch, which acted as a reference medium. Agar is widely used in microbiology as a culture medium. Agar powder with jelly strength 400 – 600 g/cm^2 by Wako Company was used for experiments. The diameters of the agar pieces were chosen to be 4 – 14 mm (s = 1, N = 0.33) to simulate T1 tumors, which are less than 20 mm. A uniform magnetic flux density of 0.1 mT was applied by the Helmholtz tri-coil and the needle tip of the sensor was inserted at 10 mm intervals hence, to the middle of agar pieces along the length (225 mm) of the magnetic fluid filled cavity tray as shown in Fig. 14. The change in signal corresponds to the difference between the signal obtained inside the magnetic fluid filled agar and the reference medium (potato starch). It can be seen from Fig. 15 that the GMR needle probe can detect magnetic fluid injected into agar pieces with a diameter as low as 4 mm. Fig. 15 shows that for a given D_w of thinned magnetic fluid the change in signal does not vary so much between the four samples (since s and N is the same) and that the signal is proportional to the weight density of thinned magnetic fluid. This means that even though the size of the cavity may change (s and N constant), the signal will only change with D_w, thus verifying equation (20). Furthermore, detection of magnetic fluid in samples with diameters as low as 4 mm shows that the GMR needle probe has a potential to be used effectively as a tool for detecting drug coupled MBs, in targeted therapy for tumors.

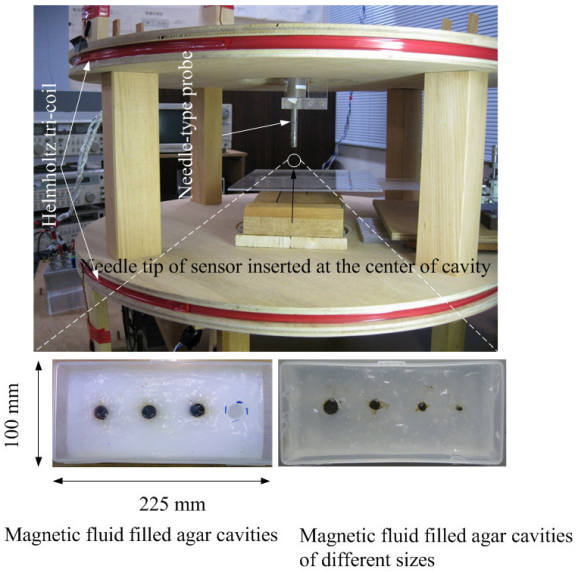

Fig. 14. Experimental setup for detecting and estimating magnetic fluid weight density inside agar cavities

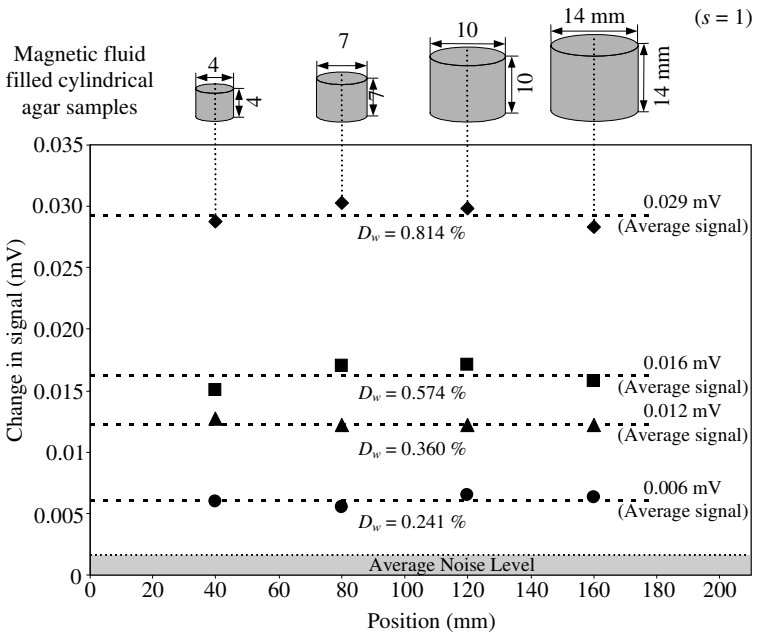

Fig. 15. Detection of magnetic fluid inside agar cavities

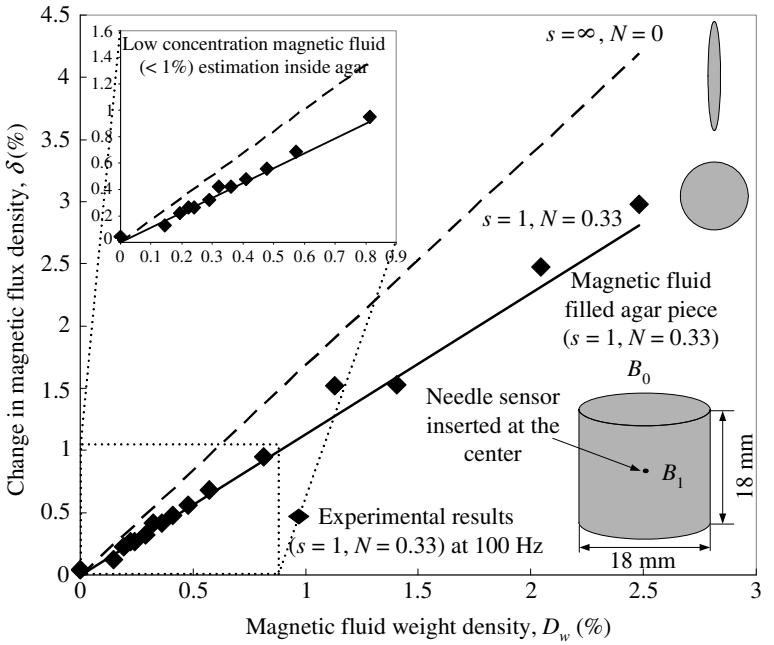

Fig. 16. Estimation of magnetic fluid weight density inside agar cavities

Since the GMR needle probe was used to successfully detect magnetic fluid inside cylindrical agar pieces of different sizes, experiments were performed to accurately estimate D_w inside cylindrical agar pieces simulating T1 tumors. One of the major obstacles for implementation of hyperthermia therapy as an effective cancer treatment is the retention of injected magnetic fluid without spreading to neighboring tissues and organs. Coupling magnetic fluid to tumor specific ligands such as antibodies, slow infiltration and repeated multi-site injections are some of the methods used to increase the retention of magnetic fluid in tumors. Experiments are performed with the GMR needle sensor to estimate D_w in 18 mm diameter agar cavities (s = 1, N = 0.33) since, to provide adequate heat to kill the tumor without affecting surrounding healthy cells, D_w needs to be confirmed before and after treatment (to check remaining density). The GMR needle was inserted at the center of the 18 mm agar cavities and B_1 and B_0 was measured simultaneously due to the bridge circuit design of the GMR needle probe. It can be seen from Fig. 16 that D_w is proportional to the change in magnetic flux density and agrees well with theoretical results obtained based on ellipsoidal cavities. Concentrations as low as 0.145 % weight density can be successfully estimated [52, 53].

2.4.3 Estimation of Magnetic Fluid Weight Density Inside Large Cylindrical Agar Cavities

In section 2.4.2 experiments were performed with agar cavities simulating T1 cancer tumors. Different size agar cavities were injected with magnetic fluid to simulate fluid

filled tumors. The GMR needle probe was then used to measure the change in magnetic flux density inside and outside the agar cavities simultaneously. The size of the tumor should be considered since out of the 20 mm needle of the GMR probe 15 mm is available to be inserted inside the tumor. Since the needle tip should be inserted at the center of the tumor where the magnetic flux density is greatest (given that the tumor is exposed to a uniform magnetic flux density), the diameter of a given tumor should be less than or equal to 30 mm. Since diameters of the cylindrical agar cavities simulating tumors in the T1 stage of cancer were less than 20 mm the needle of the GMR sensor, which is 20 mm in length, was easily inserted into the center of the agar cavities to measure magnetic flux density inside. However, in T3 and 4 stages of cancer, commonly called the "later/advanced stages" of cancer, the diameters of tumors are more than 50 mm. So, the needle cannot be inserted at the center. Hence, a new experimental method was developed to estimate D_w inside large tumors. Taking advantage of the fact that the distance between the GMR sensing area at the tip and the three other sensors near the bonding pads is 20 mm, magnetic flux density is obtained at 20 mm steps as shown in Fig. 17. The total change in magnetic flux density is calculated by summing the change in magnetic flux densities at each step as shown in the equation below.

$$B_{TotalChange} = \sum_{i=0}^{n} \left(B_{i+1} - B_i \right). \tag{21}$$

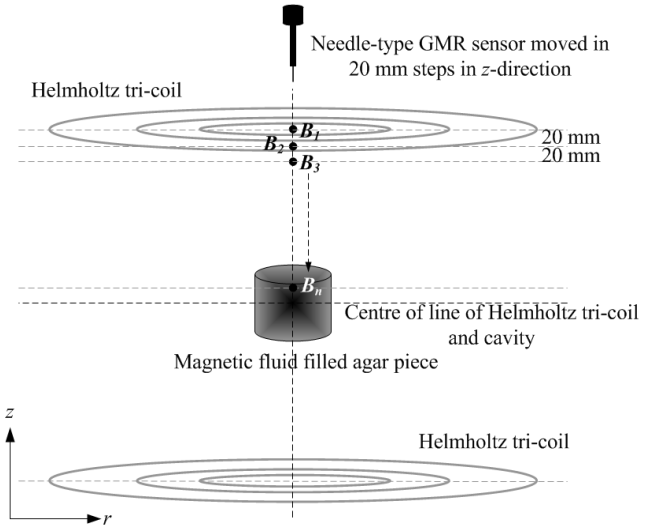

Fig. 17. Method of estimating magnetic fluid weight density inside large cavities

Figure 18 shows the comparison between the numerical and experimental results. It can be seen that if magnetic flux density can be measured at the center of the cavity, the change in magnetic flux density is approximately equal to the theoretical results. However, since the needle of the GMR probe is only 20 mm in length, the change in magnetic flux density is obtained by equation (21) for large cavities, where the needle cannot be inserted into the center of the cavity. The number of steps used in this case was 7. This meant that the needle was fully inserted in the magnetic fluid filled cavity after 7 steps, however the tip was not at the center of the cavity. It can be seen from Fig. 18 that the summing method proposed for large cavities gives a good approximation when the sensor needle cannot be inserted at the center of the cavity.

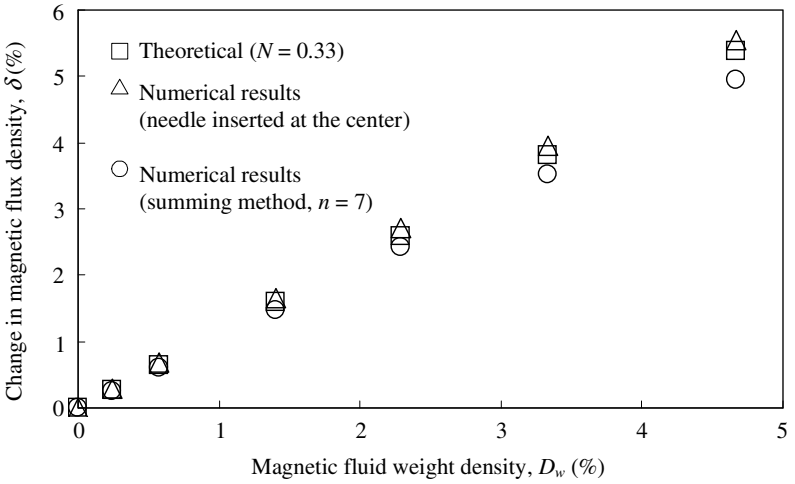

Fig. 18. Comparison of theoretical and numerical results for large cavities

The summing method was utilized to measure the change in magnetic flux density in magnetic fluid filled cylindrical agar cavities of 63 mm diameter (s = 1). 30 results were obtained in 30 seconds from the lock-in amplifier by MATLAB GUI and saved in the PC for further analysis. This method was more competent to handle the rapidly changing values of the lock-in amplifier, especially at points further away from the cavity. The average of 30 values was then taken. The experimental results are shown in Fig. 19. It can be seen that the total change in magnetic flux density increases with D_w. Moreover, the experimental results for large cavities compare favorably with theoretical results based on ellipsoidal cavities, numerical results obtained by numerical modeling and experimental results obtained for small cavities [54]. Figure 20 shows the results obtained for different size cylindrical agar cavities (s = 1) for a weight density of 2.29 %. Experiments done on smaller cavities (section 2.4.2) verified equation (21) for a range of sizes. It was shown that the change in magnetic flux density did not vary so much between different size cavities as long as s and hence N remained the same. The change in magnetic flux density only increased with D_w.

However, it must be noted that these experiments were performed with cavities smaller than 30 mm in diameter, hence allowing the insertion of the needle tip to the center of the cavity. In the experiments performed in this section the larger the cavity the further away it would be from the center of the cavity (where the magnetic flux density is the greatest) as shown in table 1. Thus, as diameter and/or height of a cavity increases (for a constant N) the total change in magnetic flux density decreases. Figure 20 compares the experimental results to numerical results. Even though the experimental results increase with the size of cavity they do not fluctuate so much compared to the numerical results.

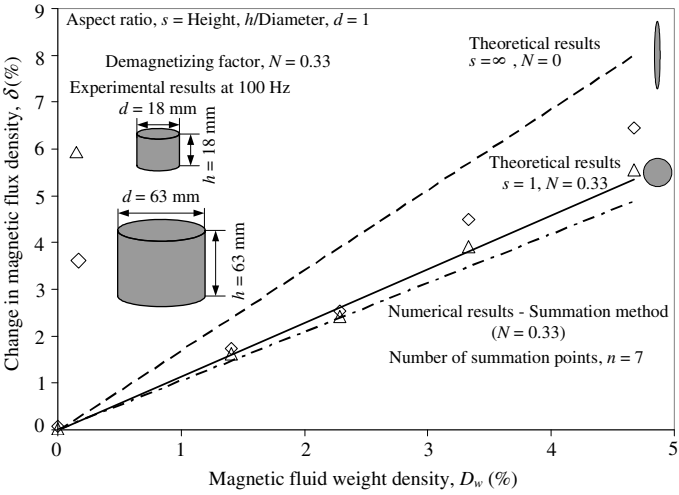

Fig. 19. Estimation of magnetic fluid weight density inside large cavities

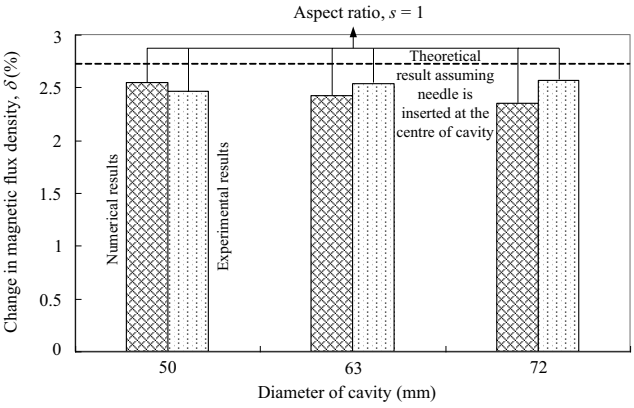

Fig. 20. Estimation of magnetic fluid weight density inside different sized cavities for D_w = 2.29 %

Table 1. Comparison of different sized cavities when needle is completely inserted inside cavity

Cavity	Diameter (mm)	Height (mm)	Distance from center of cavity to needle tip (mm)
1	50	50	10.0
2	63	63	16.5
3	72	72	21.0

2.4.4 Estimation of Very Low Concentration Magnetic Fluid Weight Density Inside Cylindrical Cavities

In section 2.4.2 experiments were performed to estimate low-concentration D_w inside cylindrical agar cavities; the limit of estimation was 0.145 %. However, estimation of very low-concentration magnetic fluid (less than 0.1 % D_w) is significant in hyperthermia therapy since the dosage is kept to a minimum *in vivo*, magnetic fluid spreads to neighboring tissue after injection which further reduces the dosage and some fluid may remain after treatment. Since successful treatment is directly proportional to D_w it is essential to estimate *in vivo*. Furthermore, current implementation of magnetic fluid based hyperthermia is in conjunction with other established forms of treatment such as radiotherapy, surgery and chemotherapy. It has been shown that cancer treatment with combination treatment is more effective compared to a given treatment on its own. However, if magnetic fluid hyperthermia therapy is to be more effective in combination treatment and also to be a feasible, stand alone, treatment there are several questions that need to be addressed. One of the main issues that need to be addressed involves the fate of magnetic fluid once used as self-heating agents in hyperthermia therapy. While it is safe to assume that only a small amount of magnetic fluid remains after treatment there is no conclusive evidence due to the novelty of magnetic fluid hyperthermia treatment. Even though, magnetic fluid is biocompatible it may be influenced by other bodily fluids or functions if it were to remain in the body for a prolonged period of time. The possible fact that magnetic fluid remains in the body for a long duration can be exploited for further treatment or for utilizing it for other applications. Remnant magnetic fluid can be moved to another part of the body by external magnetic flux gradients and reused for further/new treatment. The common factor that stands to benefit all these issues is accurate estimation of very low- concentration D_w. This section discusses the experimental apparatus fabricated and the experimental results estimating very low-concentration D_w inside agar cavities, using the GMR needle probe.

The aim of the experiments is to measure very low D_w of magnetic fluid in a cylindrical agar cavity, by measuring B_1. For this purpose a super uniform magnetic flux density generator is required for eliminating ambiguity of measurements. Since, for very low densities the percentage change in magnetic flux density is in the order of 1/10,000, it is important that the applied magnetic flux density is at least $1/10^{th}$ more uniform. For this purpose a Lee-Whiting type coil [40, 41] was designed and fabricated, producing a 0.001 % variation from the center of the coil in approximately 35 % of the outer coil spacing along the axial direction and 25 % of the diameter of

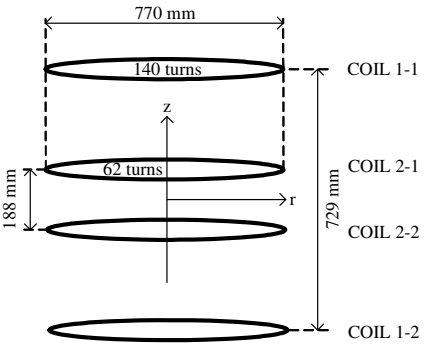

(a) Design of the Lee-Whiting coil.

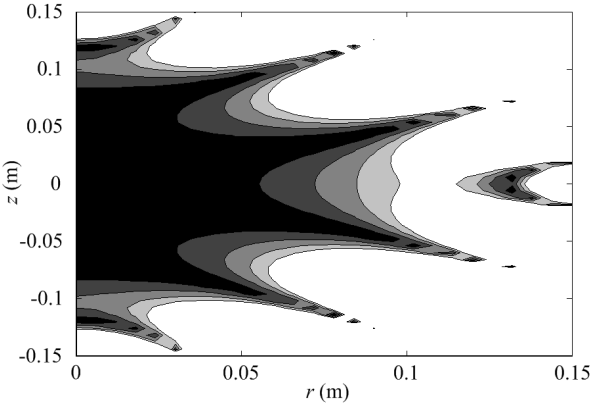

(b) Contour error plot (≤ 0.001 % fluctuation from center of the coil).

Fig. 21. Lee-Whiting coil

the coils in the radial direction. The Lee-Whiting coil design is shown in Fig. 21 (a) and the analytical results are shown in Fig. 21 (b).

Figure 22 shows the experimental setup where the fabricated Lee-Whiting coil was used to produce a uniform magnetic flux density of 0.09 mT at 50 and 100 Hz. Cylindrical agar pieces of d = 18 mm (s = 1) were injected with very low-concentration magnetic fluid (D_w = 0.03 – 0.2 %). The GMR needle probe was inserted to the center of magnetic fluid filled agar cavities. The differential magnetic flux density is in the order of nanotesla in the experimental situation. The bridge structure of the GMR needle probe measured the differential magnetic flux density simultaneously. The bridge output was amplified 100 times and sent to the lock-in amplifier. Then the data from the lock-in amplifier was transferred through GPIB to a computer for further analysis. For each low-concentration weight density, 5 values were taken and averaged. Experimental results shown in Fig. 23 indicate that the change in magnetic flux density is proportional to D_w [55]. However, the current limit of estimation has a good possibility to be influenced by the construction and coiling

errors of the Lee-Whiting coil. Shown in table 2.2 are the error percentages at 0.02 m in the axial direction if the coils or diameters are altered by ±1/2 mm as shown in Fig. 24. Also, the error percentage increases if current distribution is considered as a square as shown in Fig. 24 instead of a point (as assumed in analytical analysis).

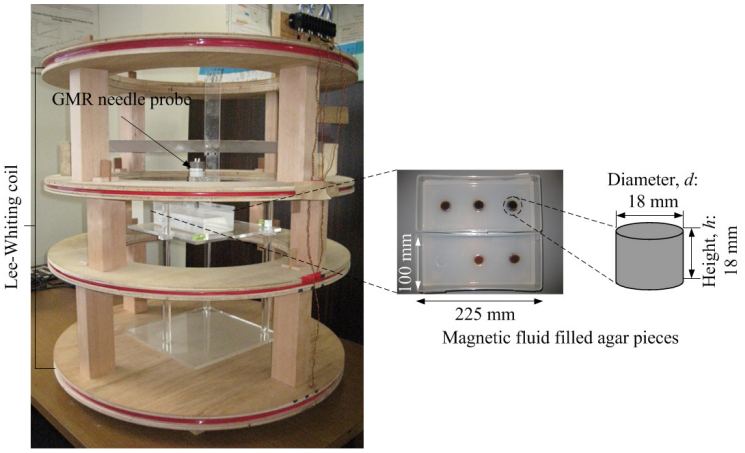

Fig. 22. Experimental setup

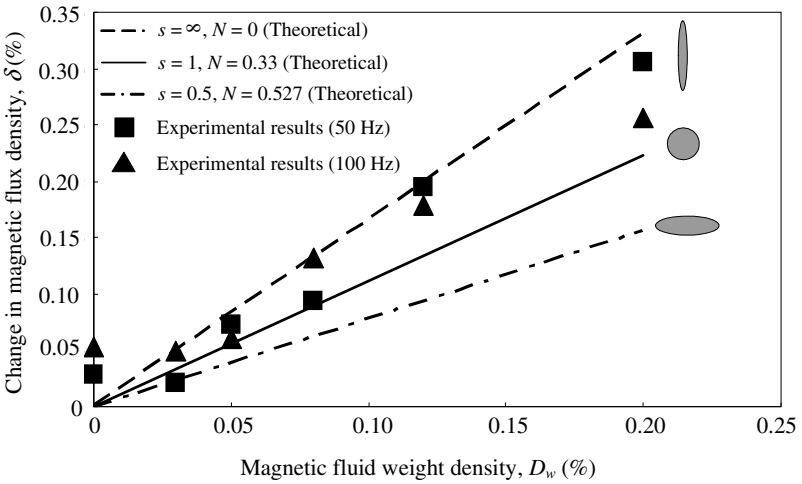

Fig. 23. Estimation of very low-concentration magnetic fluid weight density inside agar cavities

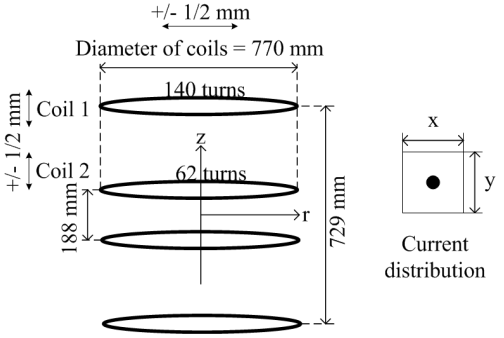

Fig. 24. Possible errors due to construction and coiling.

Table 2. Analysis of error percentages due to coiling and construction

Coil number	+1 mm (%)	-1 mm (%)	+2 mm (%)	-2 mm (%)
1_Distance	0.007	0.007	0.015	0.015
2_Distance	0.008	0.008	0.015	0.015
1_Radius	0.0037	0.0037	0.0075	0.0075
2_Radius	0.006	0.006	0.012	0.012

3 Conclusions

A novel GMR needle probe that is utilized to detect and estimate magnetic fluid weight density was reported in this section. The unique design of the fabricated GMR needle probe is especially made for application *in vivo* in a low-invasive way. A theoretical basis was obtained for detecting and estimating D_w *in vivo* based on relationships between relative permeability, weight density of magnetic fluid and magnetic flux density inside and outside a magnetic fluid filled cavity. An experimental setup (including a novel GMR needle probe, Helmholtz tri-coil and Lee-Whiting coil) and procedure with agar injected with magnetic fluid to simulate actual clinical process was developed.

Experiments were performed to detect and estimate D_w inside a variety of mediums simulating tumors, using the GMR needle probe, with the long term objective of estimating *in vivo*, especially in the area of hyperthermia therapy, a form of cancer treatment. Experiments were performed initially by inserting the GMR needle probe in a tray with magnetic fluid filled embedded cavities for confirmation of theoretical analysis. Cylindrical agar cavities simulating 1st and 2nd stage tumors were injected with magnetic fluid and the GMR needle probe was used to measure the magnetic flux density inside and outside the agar cavity. By measuring the differential magnetic flux density, D_w was estimated. The lowest D_w that could be estimated inside 18 mm diameter cylindrical agar cavities was 0.03 %. To estimate D_w in large tumors commonly found in later stages of cancer, a summing method was developed, taking into

account the distance between the sensing element at the tip of the needle and the sensing elements near the bonding pads. The lowest D_w that could be estimated inside 63 mm cylindrical agar cavities was 1.414 %. The research performed in this section shows that in the future the GMR needle probe could be used not only in hyperthermia therapy but also in other advanced medical applications.

Acknowledgment. The authors acknowledge Prof. Masayoshi Iwahara (Retired) from the Institute of Nature and Environmental Technology, Kanazawa, Japan, for his help in this research. The authors would like to thank Professor Ichiro Sasada of Kyushu University for his kind help in designing and building the Helmholtz tri-coil system. Professor Subhas Chandra Mukhopadhyay of Massey University deserves the gratitude of the authors for his valuable advice. The authors also acknowledge Mrs. Agnieszka Łekawa-Raus and Dr. Adam Kurnicki for their contributions to this research. The authors gratefully acknowledge research support from the Ministry of Education, Culture, Sports, Science and Technology (MEXT) and the Japan Society for Promotion of Science (JSPS).

References

[1] Dennis, C.L., Jackson, A.J., Borchers, J.A., Ivkov, R., Foreman, A.R., Hoopes, P.J., Strawbridge, R., Pierce, Z., Goerntiz, E., Lau, J.W., Gruettner, C.: The influence of magnetic and physiological behaviour on the effectiveness of iron oxide nanoparticles for hyperthermia. Journal of Physics D: Applied Physics 41, 134020 (2008)

[2] Hiergeist, R., Andrä, W., Buske, N., Hergt, R., Hilger, I., Richter, U., Kaiser, W.: Application of magnetic ferrofluids for hyperthermia. Journal of Magnetism and Magnetic Materials 201, 420–422 (1999)

[3] Ivkov, R., DeNardo, S.J., Daum, W., Foreman, A.R., Goldstein, R.C., Nemkov, V.S., DeNardo, G.L.: Application of High Amplitude Alternating Magnetic Fields for Heat Induction of Nanoparticles Localized in Cancer. Clinical Cancer Research 11, 7093s–7103s (2005)

[4] Jordan, A., Scholz, R., Wust, P., Schirra, H., Schiestel, T., Schmidt, H., Felix, R.: Endocytosis of dextran and silan-coated magnetite nanoparticles and the effect of intracellular hyperthermia on human mammary carcinoma cells in vitro. Journal of Magnetism and Magnetic Materials 194, 185–196 (1999)

[5] Sincai, M., Ganga, D., Ganga, M., Argherie, D., Bica, D.: Antitumor effect of magnetite nanoparticles in cat mammary adenocarcinoma. Journal of Magnetism and Magnetic Materials 293, 438–441 (2005)

[6] Şincai, M., Gânga, D., Bica, D., Vékás, L.: The antitumor effect of locoregional magnetic cobalt ferrite in dog mammary adenocarcinoma. Journal of Magnetism and Magnetic Materials 225, 235–240 (2001)

[7] Wada, S., Tazawa, K., Suzuki, N., Furuta, I., Nagano, I.: Pulp ablation therapy by inductive heating: heat generation characteristics in the pulp cavity. Oral Diseases 13, 193–197 (2007)

[8] Wilhelm, C., Gazeau, F.: Magnetic nanoparticles: Internal probes and heaters within living cells. Journal of Magnetism and Magnetic Materials 321, 671–674 (2009)

[9] Storm, F.K., Harrison, W.H., Elliot, R.S., Morton, D.L.: Normal Tissue and Solid Tumor Effects of Hyperthermia in Animal Models and Clinical Trials. Cancer Research 39, 2245–2251 (1979)
[10] Atsumi, T., Jeyadevan, B., Sato, Y., Tohji, K.: Heating efficiency of magnetite particles exposed to AC magnetic field. Journal of Magnetism and Magnetic Materials 310, 2841–2843 (2007)
[11] Bae, S., Lee, S.W.: Applications of $NiFe_2O_4$ nanoparticles for a hyperthermia agent in biomedicine. Applied Physics Letters 89, 252503 (2006)
[12] Bae, S., Lee, S.W., Takemura, Y., Yamashita, E., Kunisaki, J., Zurn, S., Kim, C.S.: Dependence of Frequency and Magnetic Field on Self-Heating Characteristics of $NiFe_2O_4$ Nanoparticles for Hyperthermia. IEEE Transactions on Magnetics 42, 3566–3568 (2006)
[13] Gilchrist, R.K., Medal, R., Shorey, W.D., Hanselman, R.C., Parrott, J.C., Taylor, C.B.: Selective Inductive Heating of Lymph Nodes. Annals of Surgery 146, 596–606 (1957)
[14] Pankhurst, Q.A., Connolly, J., Jones, S.K., Dobson, J.: Applications of magnetic nanoparticles in biomedicine. Journal of Physics D: Applied Physics 36, R167–R181 (2003)
[15] Goodwin, S., Peterson, C., Hoh, C., Bittner, C.: Targeting and retention of magnetic targeted carriers (MTCs) enhancing intra-arterial chemotherapy. Journal of Magnetism and Magnetic Materials 194, 132–139 (1999)
[16] Jurgons, R., Seliger, C., Hilpert, A., Trahms, L., Odenbach, S., Alexiou, C.: Drug loaded magnetic nanoparticles for cancer therapy. Journal of Physics: Condensed Matter 18, S2893–S2902 (2006)
[17] Berry, C.C., Curtis, A.S.G.: Functionalisation of magnetic nanoparticles for applications in biomedicine. Journal of Physics D: Applied Physics 36, R198–R206 (2003)
[18] Ramanujan, R.V.: Clinical Applications of Magnetic Nanomaterials. In: Proceedings of the First International Bioengineering Conference, Singapore, pp. 174–177 (2004)
[19] Andrés Vergés, M., Costo, R., Roca, A.G., Marco, J.F., Goya, G.F., Serna, C.J., Morales, M.P.: Uniform and water stable magnetite nanoparticles with diameters around the monodomain-multidomain limit. Journal of Physics D: Applied Physics 41, 134003 (2008)
[20] Gupta, A.K., Gupta, M.: Synthesis and surface engineering of iron oxide nanoparticles for biomedical applications. Biomaterials 26, 3995–4021 (2005)
[21] Tartaj, P., del Puerto Morales, M., Veintemillas-Verdaguer, S., González-Carreño, T., Serna, C.J.: The preparation of magnetic nanoparticles for applications in biomedicine. Journal of Physics D: Applied Physics 36, R182–R197 (2003)
[22] Park, S.I., Kim, J.H., Kim, C.G., Kim, C.O.: Size-controlled magnetic nanoparticles with lecithin for biomedical applications. Journal of Magnetism and Magnetic Materials 312, 386–389 (2007)
[23] Dutz, S., Andrä, W., Hergt, R., Müller, R., Oestreich, C., Schmidt, C., Töpfer, J., Zeisberger, M., Bellemann, M.E.: Influence of dextran coating on the magnetic behaviour of iron oxide nanoparticles. Journal of Magnetism and Magnetic Materials 311, 51–54 (2007)
[24] Uozumi, Y., Tonohata, N., Imamura, M.: Magnetic Fluid Behaviour under External Fields in View of Medical Applications. In: Second International Conference on Innovative Computing, Information and Control, September 5-7, p. 370 (2007), doi:10.1109/ICICIC.2007.373
[25] Andrés Vergés, M., Costo, R., Roca, A.G., Marco, J.F., Goya, G.F., Serna, C.J., Morales, M.P.: Uniform and water stable magnetite nanoparticles with diameters around the monodomain-multidomain limit. Journal of Physics D: Applied Physics 41, 134003 (2008)
[26] Bahadur, D., Giri, J.: Biomaterials and magnetism. Sādhanā 28(3,4), 639–656 (2003)

[27] Duguet, E., Vasseur, S., Mornet, S., Goglio, G., Demourgues, A., Portier, J., Grasset, F., Veverka, P., Pollert, E.: Towards a versatile platform based on magnetic nanoparticles for in vivo applications. Bulletin of Materials Science 29, 581–586 (2006)
[28] Józefczak, A., Skumiel, A.: Study of heating effect and acoustic properties of dextran stabilized magnetic fluid. Journal of Magnetism and Magnetic Materials 311, 193–196 (2007)
[29] Hergt, R., Dutz, S.: Magnetic particle hyperthermia-biophysical limitations of a visionary tumour therapy. Journal of Magnetism and Magnetic Materials 311, 187–192 (2007)
[30] Jordan, A., Scholz, R., Maier-Hauff, K., Johannsen, M., Wust, P., Nadobny, J., Schirra, H., Schmidt, H., Deger, S., Loening, S., Lanksch, W., Felix, R.: Presentation of a new magnetic field therapy system for the treatment of human solid tumors with magnetic fluid hyperthermia. Journal of Magnetism and Magnetic Materials 225, 118–126 (2001)
[31] Jordan, A., Scholz, R., Wust, P., Fähling, H., Felix, R.: Magnetic fluid hyperthermia (MFH): Cancer treatment with AC magnetic field induced excitation of biocompatible superparamagnetic nanoparticles. Journal of Magnetism and Magnetic Materials 201, 413–419 (1999)
[32] Yamada, S., Chomsuwan, K., Mukhopadhyay, S.C., Iwahara, M., Kakikawa, M., Nagano, I.: Detection of magnetic fluid volume density with a GMR sensor. Journal of the Magnetics Society of Japan 31, 44–47 (2007)
[33] Mukhopadhyay, S.C., Chomsuwan, K., Gooneratne, C.P., Yamada, S.: A Novel Needle-Type SV-GMR Sensor for Biomedical Applications. IEEE Sensors Journal 7, 401–408 (2007)
[34] Yamada, S., Gooneratne, C.P., Chomsuwan, K., Iwahara, M., Kakikawa, M.: Estimation of Low-Concentration Magnetic Fluid Density with GMR Sensor. Review of Progress in Quantitative Nondestructive Evaluation 975, 873–880 (2008)
[35] Gooneratne, C., Lekawa, A., Iwahara, M., Kakikawa, M., Yamada, S.: Estimation of Low Concentration Magnetic Fluid Weight Density and Detection inside an Artificial Medium Using a Novel GMR Sensor. Sensors and Transducers Journal 90, 27–38 (2008)
[36] Gooneratne, C., Chomsuwan, K., Łękawa, A., Kakikawa, M., Iwahara, M., Yamada, S.: Estimation of Density of Low-Concentration Magnetic Fluid by a Needle-Type GMR Sensor for Medical Applications. Journal of the Magnetics Society of Japan 32, 191–194 (2008)
[37] Bozorth, R.M.: Ferromagnetism, 5th edn. New Jersey, Van Nostrand (1951)
[38] Bronaugh, E.L.: Helmholtz Coils for Calibration of Probes and Sensors: Limits of Magnetic Field Accuracy and Uniformity. In: Proceedings of the IEEE International Symposium on Electromagnetic Compatibility, Atlanta, U.S.A (1995)
[39] Wang, J., She, S., Zhang, S.: An improved Helmholtz coil and analysis of its magnetic field homogeneity. Review of Scientific Instruments 73, 2175–2179 (2002)
[40] Kirschvink, J.L.: Uniform Magnetic Fields and Double-Wrapped Coil Systems. Bioelectromagnetics 13, 401–411 (1992)
[41] Gottardi, G., Mesirca, P., Agostini, C., Remondini, D., Bersani, F.: A Four Coil Exposure System (Tetracoil) Producing a Highly Uniform Magnetic Field. Bioelectromagnetics 24, 125–133 (2003)
[42] Caprari, R.S.: Optimal current loop systems for producing uniform magnetic fields. Measurement Science and Technology 6, 593–597 (1995)
[43] Schill Jr., R.A., Hoff, K.: Characterizing and calibrating a large Helmholtz coil at low ac magnetic field levels with peak magnitudes below the earth's magnetic field. Review of Scientific Instruments 72, 2769–2776 (2001)

[44] Lee, S.G., Kang, C.S., Chang, J.W.: A square-loop Helmholtz coil system for the evaluation of a single-layer second-order high- it T_c SQUID gradiometer. Physica C 460-462, 1472–1474 (2007)
[45] Alamgir, A.K.M., Fang, J., Gu, C., Han, Z.: Square Helmholtz coil with homogenous field for magnetic measurement of longer HTS tapes. Physica C 424, 17–24 (2005)
[46] Lüdke, J., Ahlers, H., Albrecht, M.: Novel Compensated Moment Detection Coil. IEEE Transactions on Magnetics 43, 3567–3572 (2007)
[47] Sasada, I., Nakashima, Y.: A planar coil system consisting of three coil pairs for producing uniform magnetic field. Journal of Applied Physics 99, 08D904-08D904-3 (2006)
[48] TNM classification of malignant tumors, http://www.uicc.org/tnm
[49] Miyagawa, T., Shimazui, T., Hinotsu, S., Oikawa, T., Sekido, N., Miyanaga, N., Kawai, K., Akaza, H.: Does Tumor Size or Microvas-cular Invasion Affect Prognosis in Patients with Renal Cell Carcinoma? Japan Journal of Clinical Oncology 37, 197–200 (2007)
[50] Lugli, A., Zlobec, I., Singer, G., Lugli, A.K., Terracciano, L.M., Genta, R.M.: Napoleon Bonaparte's gastric cancer: a clinicopathologic approach to staging, pathogenesis, and etiology. Nature Clinical Practice Gastroenterology and Hepatology 4, 52–57 (2007)
[51] Hilger, I., Hert, R., Kaiser, W.A.: Towards breast cancer treatment by magnetic heating. Journal of Magnetism and Magnetic Materials 293, 314–319 (2005)
[52] Yamada, S., Gooneratne, C.P., Iwahara, M., Kakikawa, M.: Detection and Estimation of Low-Concentration Magnetic Fluid Inside Body by a Needle-Type GMR Sensor. IEEE Transactions on Magnetics 44, 4541–4544 (2008)
[53] Gooneratne, C.P., Kakikawa, M., Iwahara, M., Yamada, S.: GMR Sensor Application in Detecting and Estimating Magnetic Fluid Weight Density inside Various Size Tumors. Journal of the Magnetics Society of Japan 33, 175–178 (2009)
[54] Gooneratne, C.P., Kurnicki, A., Iwahara, M., Kakikawa, M., Mukhopadhyay, S.C., Yamada, S.: A GMR Needle Probe to Estimate Magnetic Fluid Weight Density Inside Large Tumors. In: Mukhopadhyay, S.C., Gupta, G.S., Huang, R.Y.-M. (eds.) Recent Advances in Sensing Technology. LNEE, vol. 49, pp. 1–14. Springer, Heidelberg (2009)
[55] Gooneratne, C.P., Kakikawa, M., Ueno, T., Yamada, S.: Measurement of Minute Changes in Magnetic Flux Density by Means of a Novel GMR Needle Probe for Application in Hyperthermia Therapy. Journal of the Magnetics Society of Japan 34, 119–122 (2010)